Dalton Transactions

Cite this: *Dalton Trans.*, 2012, **41**, 4833

www.rsc.org/dalton

PAPER

Strong π-delocalization and substitution effect on electronic properties of dithienylpyrrole-containing bipyridine ligands and corresponding ruthenium complexes†

Sajida Noureen,[a] Stefano Caramori,[b] Antonio Monari,[c] Xavier Assfeld,[c] Roberto Argazzi,[b] Carlo A. Bignozzi,[b] Marc Beley[a] and Philippe C. Gros*[a]

Received 7th December 2011, Accepted 24th January 2012
DOI: 10.1039/c2dt12367c

The first dithienylpyrrole (DTP)-based bipyridine ligands has been prepared and coordinated with ruthenium to give the corresponding homoleptic complexes. Bipyridine was bound at pyrrole (DTP_1) or thiophene (DTP_2) ring. A strong bathochromic effect was obtained by switching from pyrrole to thiophene for ligands and complexes. Interestingly the DTP_2 series offered a wide absorption window from UV to visible domain with an almost constant absorbance. These effects are due to a larger extent of delocalization as supported by DFT calculations and photophysical measurements.

Introduction

Ruthenium–polypyridine complexes are highly important coordination compounds due to their unique photophysical and redox properties as well as electron transfer and light harvesting ability.[1–4] As a consequence of these features, ruthenium complexes rapidly became ideal candidates for photosensitization in several applications exploiting light energy such as dye-sensitized solar cells,[5–8] switches,[9,10] or molecular engines.[11–13] The efficiency of these devices is highly dependent on the complexes' ability to strongly absorb the sunlight in a large domain, ideally from the UV to NIR range. This is made possible by a metal-to-ligand charge transfer (MLCT) occurring between ruthenium and the ancillary ligands at low energy. The energetic level of the MLCT can be tuned and drawn to lower values by modifying the ligand structure or its substitution. Bipyridines bearing π-delocalized moieties have been found to be efficient for this purpose[14–16] also allowing a concomitant increase of the molar extinction coefficient. Our group has shown recently that 2,2′-bipyridines bearing pyrrole-based π-extended moieties brought interesting properties to ruthenium complexes such as wide absorption range and good performance in dye-sensitized solar cells.[17–19] With the aim to further extend electron delocalization in the compounds above, we decided to examine the effect of mixed pyrrole-based oligomers moieties. Despite better oxidation capability and enhanced luminescence properties,[20,21] 2,5-dithienylpyrrole (DTP) has been less studied[22–25] and used for organic electronic applications than oligothiophenes essentially due to lack of efficient synthetic routes. In addition, in contrast with oligothiophenes[26,27] and oligopyrroles,[28,29] the DTP moieties have not been bound to a bipyridine ligand yet and their effect on the electronic properties of the corresponding complexes remains underexplored. Herein we report the synthesis of a range of new DTP-based bipyridine ligands and their corresponding homoleptic ruthenium complexes (Fig. 1) as well as their characterization. A dramatic substituent effect has been observed for the **DTP_2** series (bound to bipyridine *via* its thiophen ring) and their corresponding complexes leading to a marked bathochromic effect with strong increase of absorption in the visible domain. This effect on ligands and complexes is discussed on the basis of transient spectroscopy as well as density functional (DFT) and time dependent density functional (TD-DFT) theory calculations.[30–36]

Results and discussion

1. Ligands and complexes synthesis

The synthetic strategy to access the bipyridine ligands was based on the Wadsworth–Emmons reaction between a bipyridine diphosphonate and aldehydes to create the styryl link needed to ensure efficient electronic communication between the DTP moiety and bipyridine and metal center in the complex. Thus we had to prepare various DTP-based compounds bearing carboxaldehyde functions at various positions *i.e.* on the thiophene and the pyrrole ring (Scheme 1). The DTP moiety was built using

[a]*Groupe SOR, SRSMC, Université de Lorraine, CNRS, Faculté des Sciences, Boulevard des Aiguillettes, F-54506 Vandoeuvre-Lès-Nancy, France. E-mail: philippe.gros@srsmc.uhp-nancy.fr; Fax: +33(0) 383684785; Tel: +33(0)383684979*
[b]*Chemistry Department, University of Ferrara, Via Luigi Borsari 46, 44100 Ferrara, Italy. E-mail: cte@unif.it; Fax: +39.0532.240709; Tel: +39 0532 291163*
[c]*Equipe CBT, SRSMC, Université de Lorraine, CNRS, Faculté des Sciences, Boulevard des Aiguillettes, F-54506 Vandoeuvre-Lès-Nancy, France. E-mail: antonio.monari@cbt.uhp-nancy.fr; Fax: +33(0) 383684371; Tel: +33(0)383684380*
†Electronic supplementary information (ESI) available. See DOI: 10.1039/c2dt12367c

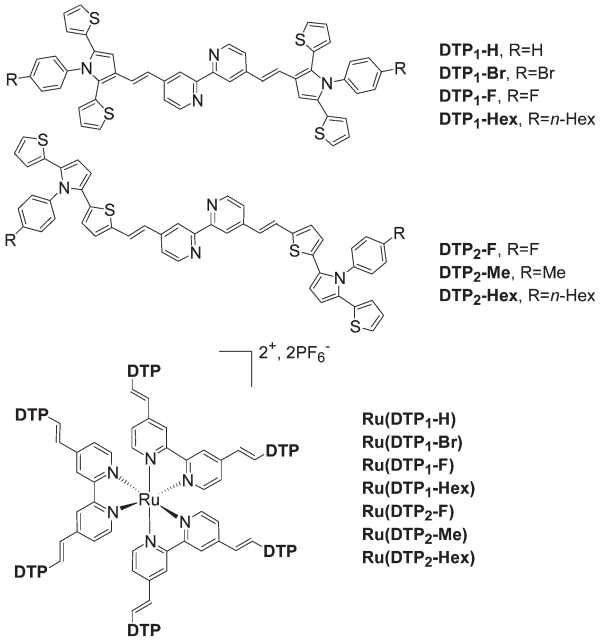

Fig. 1 DTP-based ligands and complexes studied in this work.

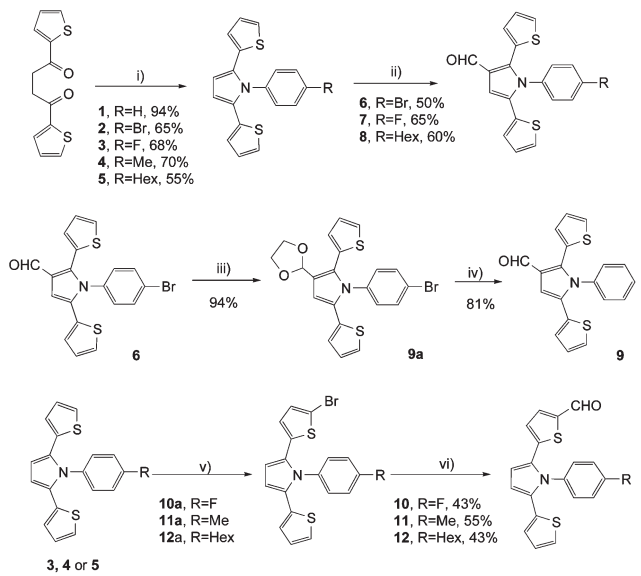

Scheme 1 Preparation of DTP-based aldehydes. *Reagents and conditions*: (i) aniline (4 equiv.), AcOH–toluene, reflux (24 h). (ii) $POCl_3$ (4 equiv.), DMF, r.t. (12 h) then 70 °C (1h). (iii) 1,2-ethanediol, APTS (2.5%), toluene, reflux (12 h). (iv) (1) n-BuLi (1 equiv.), THF, −78 °C (0.5 h); (2) H_2O; (3) APTS (1.2 equiv.), acetone, 4-picoline (1 equiv.), toluene reflux, (24 h). (v) NBS, (1 equiv.), $CHCl_3$/EtCOOH (10 : 1), −50 °C (1.5 h). (vi) (1) n-BuLi (1 equiv.), THF, −40 °C (1 h); (2) DMF (1.5 equiv., −78 °C then r.t.

the Paal–Knorr reaction between substituted anilines and 1,4-dithienyl-butanedione.[37] Among several conditions tried, the use of acetic acid in refluxing toluene was retained, giving the expected compounds **1**–**5**[38] in 55–94% yield. The Vilsmeier–Haack formylation was first chosen to next introduce the carboxaldehyde, which was introduced exclusively on the pyrrole ring from **2**, **3** and **5** leading to **6**, **7** and **8**, respectively, in acceptable yields. When **1** was reacted under the same conditions, an inseparable mixture containing aldehyde **9** as revealed by ^{1}H NMR of the crude product. A selective route to **9** was next found using **6** as precursor. The aldehyde was first protected as a dioxolane and the bromine was removed by treatment with BuLi. After deprotection under acidic conditions, **9** was obtained in 81% yield.

Table 1 Preparation of ligands and ruthenium complexes

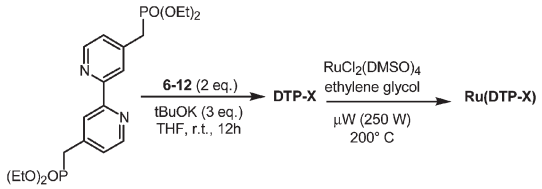

Aldehyde	**DTP-X**, yield (%)	**Ru(DTP-X)**, yield (%)
9	**DTP_1-H**, 68	**Ru(DTP_1-H)**, 76
6	**DTP_1-Br**, 38	**Ru(DTP_1-Br)**, 79
7	**DTP_1-F**, 31	**Ru(DTP_1-F)**, 75
8	**DTP_1-Hex**, 36	**Ru(DTP_1-Hex)**, 63
10	**DTP_2-F**, 73	**Ru(DTP_2-F)**, 65
11	**DTP_2-Me**, 46	**Ru(DTP_2-Me)**, 40
12	**DTP_2-Hex**, 40	**Ru(DTP_2-Hex)**, 66

Finally, we investigated the introduction of the aldehyde function on the thiophene ring in **3**, **4** and **5** using a bromination–lithiation sequence. The monobromination occurred mainly on the thiophene ring using 1 equiv. of NBS at −50 °C in the presence of propionic acid. Further bromine lithium exchange was performed using BuLi and the lithiated compound treated with DMF leading to **10**, **11** and **12** in 43, 55 and 43% yield, respectively. With aldehydes **6–12** in hand, we turned to the preparation of the DTP-based bipyridine ligands. The Wadsworth–Emmons reaction between bipyridine diphosphonate and aldehydes was investigated. The bipyridine diphosphonate was prepared in 3 steps from 4,4′-dimethyl-2,2′- bipyridine using the Fraser's procedure.[39,40] Reaction with 2 equiv. of aldehyde under basic conditions gave the expected ligands (Table 1). The symmetrically coordinated complexes **Ru(DTP-X)** were then prepared by reacting $RuCl_2(DMSO)_4$ with 3 equiv. of ligand under microwave irradiation. The complexes were obtained in good yield after 10 min of stirring.

The new compounds were next characterized by UV-vis spectroscopy and electrochemistry in order to measure the effect of DTP on electronic properties (Tables 2 and 3).

2. Characterization of ligands

As shown in Fig. 2, ligands of the **DTP_1-X** series bound to the styryl–bipyridine through the pyrrole ring exhibited absorption spectra with a similar shape. An intense band was observed near 310 nm and another with a lower intensity in the 350–384 nm range. A significant red-shift was observed with **DTP_1-Hex** bearing the electron-donating hexyl group (λ_{abs} = 384 nm instead of 350–360 nm for the other ligands). The ε values were found to be dependent on the substitution, the best absorption was obtained for **DTP_1-Br** and the lowest for **DTP_1-Hex**. Surprisingly, unsubstituted **DTP_1-H** and **DTP_1-F** bearing the most

electron-withdrawing fluorine group gave almost the same ε values.

Absorption spectra of the **DTP$_2$-X** series strongly contrasted with those of the **DTP$_1$-X** one since a strong bathochromic effect toward the visible domain was observed (λ_{max} = 433, 435 and 439 nm for **DTP$_2$-F**, **DTP$_2$-Me** and **DTP$_2$-Hex** respectively). Furthermore, the absorption of high intensity near 305 nm observed with the other ligands was dramatically weakened.

Table 2 Photophysical and electrochemical properties of ligands

Ligand	$\lambda_{abs\text{-}max}$ (nm)[a] (ε (10^3 L M^{-1} cm^{-1}))	$\lambda_{em\text{-}max}$[b] ($\lambda_{exc.}$) (nm)	E_{pa}[c] (L^+/L) (V/SCE)	E_{pc}[d] (L/L^-) (V/SCE)
DTP$_1$-H	352 (42.1)	542 (352)	1.02 (irrev.)	−1.90 (irrev.)
	311 (53.9)	542 (311)	—	—
DTP$_1$-Br	356 (42.4)	531 (356)	0.98 (irrev.)	−1.90 (irrev.)
	309 (61.0)	—	—	—
DTP$_1$-F	360 (39.0)	—	1.0 (irrev.)	−1.94 (irrev.)
	310 (52.5)	540 (310)	—	—
DTP$_1$-Hex	381 (26.0)	540 (381)	0.96 (irrev.)	−1.92 (irrev.)
	304 (41.6)	540 (304)	—	—
DTP$_2$-F	432 (59.5)	575 (432)	0.84 (irrev.)	−1.63 (irrev.)
	316 (24.9)	575 (316)	—	—
DTP$_2$-Me	435 (48.2)	580 (435)	0.80 (irrev.)	−1.65 (irrev.)
	318 (19.1)	—	—	—
DTP$_2$-Hex	439 (56.1)	580 (438)	0.84 (irrev.)	−1.65 (irrev.)
	323 (27.5)	580 (322)	—	—

[a] Measured in DMSO at 25 °C. [b] Photomultiplier corrected emission maxima for the complexes in DMSO in the absence of O_2, A < 0.05. [c, d] First oxidation and reduction potentials, respectively, standardized with Fc^+–Fc as internal standard and converted into SCE scale by adding 0.47 V ($E_{1/2}$ Fc^+–Fc). Recorded in DMF using $Bu_4N^+PF_6^-$ as supporting electrolyte at 100 mV s^{-1}.

Such an ε increase could be assigned to an increase of the molecule dipolar moment by the electron withdrawing fluorine group. All the ligands were found emissive (see Table 2). λ_{em} for **DTP$_1$-X** were found in the 530–540 nm range while in agreement with absorption, a notable red-shift was observed with **DTP$_2$-X** (λ_{em} = 580 nm for **DTP$_2$-Hex**). Thus the way the DTP moiety was attached to bipyridine dramatically affected the electronic properties of the corresponding ligand. This probably resulted from differences in π delocalization extent in the ligands. Indeed in the case of **DTP$_2$-X** where DTP was bound by the thiophene ring a more extended delocalization was offered. In contrast, in **DTP$_1$-X** the thiophene ring did not seem to participate to the delocalization. In order to analyze the molecular structure and electron distribution into the ligands, *ab initio* calculations were performed. All the ligand geometries have thus been optimized at DFT level using B3LYP[41] exchange

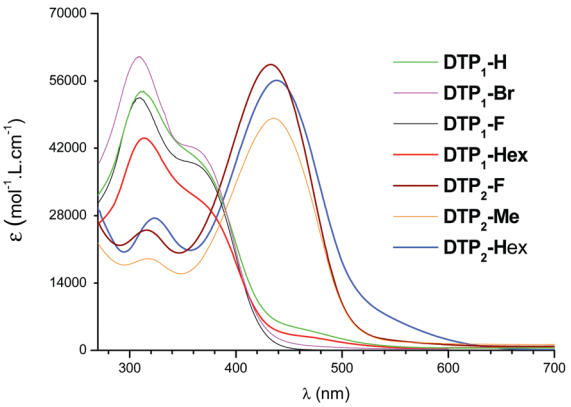

Fig. 2 Absorption spectra of ligands in DMSO.

Table 3 Photophysical and electrochemical properties of complexes

Complex	$\lambda_{abs\text{-}max}$[a] (nm) (ε(10^3 L M^{-1} cm^{-1}))	$\lambda_{em\text{-}max}$[b] (ligand based) or (MLCT)	$\tau_{singlet}$[c] (ns) $\tau_{triplet}$ (ns)	$E_{1/2}$ Ru^{III}–Ru^{II}[d] (V/SCE)	E_{pa}[d] (L^+/L) (V/SCE)	$E_{1/2}$[e] (L/L^-) (V/SCE)
Ru(DTP$_1$-H)	495 (50)	550 (ligand)	1.23	1.05 (ΔE_p = 0.18)	1.17 (irrev.)	−1.16 (ΔE_p = 0.08)
	396 (62.2)	687 (MLCT)	215	—	—	—
	308 (132.8)	—	—	—	—	—
Ru(DTP$_1$-Br)	488 (33.1)	541 (ligand)	1.64	0.98 (ΔE_p = 0.20)	0.95 (irrev.)	−1.17 (ΔE_p = 0.08)
	390 (46.6)	691 (MLCT)	217	—	—	—
	264 (112.5)	—	—	—	—	—
Ru(DTP$_1$-F)	490 (20.3)	476 (ligand)	1.57	0.98 (ΔE_p = 0.24)	1.07 (irrev.)	−1.17 (ΔE_p = 0.08)
	398 (28.2)	698 (MLCT)	212	—	—	—
	306 (64.4)	—	—	—	—	—
Ru(DTP$_1$-Hex)	489 (48.3)	541 (ligand)	1.68	0.96 (ΔE_p = 0.20)	1.00 (irrev.)	n.d.[f]
	397 (63.1)	692 (MLCT)	220	—	—	—
	306 (48.3)	—	—	—	—	—
Ru(DTP$_2$-F)	508 (72.7)	512 (ligand)	2.01	0.80 (ΔE_p = 0.120)	0.86 (irrev.)	−1.07 (ΔE_p = 0.08)
	452 (72.3)	No MLCT emission	200	—	—	—
Ru(DTP$_2$-Me)	512 (67.9)	554 (ligand)	0.58	0.77 (ΔE_p = 0.120)	0.82 (irrev.)	−1.10 (ΔE_p = 0.08)
	451 (62.5)	No MLCT emission	200	—	—	—
Ru(DTP$_2$-Hex)	513 (78.3)	577 (ligand)	0.56	0.76 (ΔE_p = 0.120)	0.82 (irrev.)	−1.11 (ΔE_p = 0.08)
	443 (75.9)	No MLCT emission	155	—	—	—
	360 (62.7)	—	—	—	—	—

[a] Measured in CH_3CN at 25 °C. [b] Photomultiplier corrected emission maxima for the complexes in DMF A < 0.05. [c] Ligand based singlet emission lifetime measured by TCSPC and triplet absorption lifetime upon 532 nm nanosecond (FWHM 7 ns) laser excitation. All measurements performed in deaerated DMF. [d] Oxidation potentials standardized with Fc^+–Fc as internal standard and converted into SCE scale by adding 0.47 V ($E_{1/2}$ Fc^+–Fc). Recorded in DMF using $Bu_4N^+PF_6^-$ as supporting electrolyte at 100 mV s^{-1}. [e] First reduction potential. [f] n.d. = not detected.

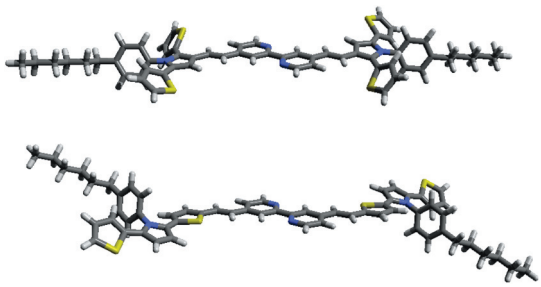

Fig. 3 TDDFT optimized geometry of **DTP$_1$-Hex** (top) and **DTP$_2$-Hex** (bottom).

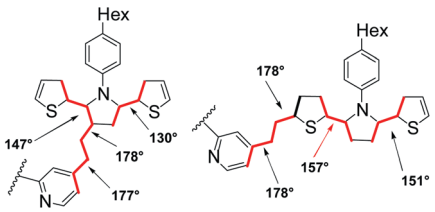

Fig. 4 Calculated dihedral angles in **DTP$_1$-Hex** (left) and **DTP$_2$-Hex** (right). Half the molecule is depicted.

correlation functional. A double zeta 6-31G[42] basis was used throughout. In order to assure a proper comparison we computed all the possible systems obtained from **DTP$_1$** and **DTP$_2$** moieties, making a total of 10 ligands. Optimized geometries for **DTP$_1$-Hex** and **DTP$_2$-Hex** are given in Fig. 3.

Dihedral angles between relevant pyrrole and thiophene rings were measured from the optimized structures (Fig. 4). In **DTP$_1$-Hex**, the bipyridine–styryl–pyrrole sequence was found to be coplanar, while thiophene rings were distorted from the plane. The styryl moiety appeared to induce a beneficial effect on the dihedral angle with regard to planarity when thiophene was bound at the *ortho* position (147° *vs*. 130° for the thiophene at the *meta* position). Thus, one thiophene could be expected to participate in the π-delocalization process. In **DTP$_2$-Hex**, the loss of planarity was minimized when a thiophene was bound to both styryl and pyrrole (θ = 157°). This was in agreement with a more extended delocalized system and favoured absorption at the lower energy domain.

The 25 first excited states have been computed by using TDDFT formalism for all the optimized ligands. CAM-B3LYP[43] functional has been used in order to better account for the long range corrections, a slightly larger augmented and polarized double zeta basis (6-31+G(d,p)[42]) has been used. The solvatochromic effect of the solvent has been taken into account by using the continuum PCM model.[44] Note that the transoid structure presented in Fig. 3 appeared as the most stable ones in solution, anyway the computed cisoid structure spectra showed only a very slight deviation from the previous ones. Computed UV-vis spectra wavelengths and oscillator strength are reported in Table 4. A fairly good agreement between experiment and theory was observed (see Table 4).

The **DTP$_2$** structures confirmed the presence of a very important red-shift of about 80 nm as compared to **DTP$_1$**. On the other hand, the different members of the same family give quite reproducible spectra, confirming the small influence of the phenyl

Table 4 Ligands TDDFT computed principal excitation wavelengths and oscillator strength

X	DTP$_1$-X λ^a (nm), (f)	DTP$_2$-X λ^a (nm), (f)
H	355.51 (2.06)	433.66 (3.52)
	318.48 (1.56)	318.44 (0.07)
	—	286.07 (0.56)
Br	351.76 (2.20)	429.08 (3.51)
	342.40 (0.01)	316.79 (0.06)
	315.43 (1.02)	285.19 (0.55)
F	352.08 (2.11)	433.61 (3.52)
	342.72 (0.01)	318.44 (0.07)
	315.52 (0.93)	286.07 (0.56)
Me	355.77 (2.11)	433.61 (3.52)
	346.33 (0.05)	318.44 (0.07)
	318.56 (1.01)	286.07 (0.56)
Hex	355.79 (2.16)	437.65 (3.55)
	346.34 (0.01)	316.73 (3.13)
	318.60 (1.13)	287.91 (0.48)

[a] Oscillator strength in parentheses.

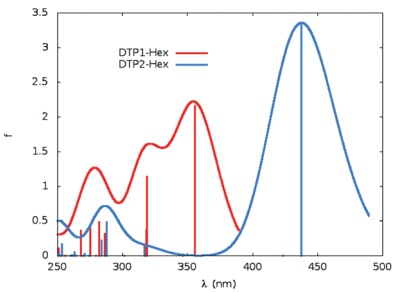

Fig. 5 Computed spectra of **DTP$_1$-Hex** and **DTP$_2$-Hex**.

substituent as expected from its pseudo-orthogonality with regard to the pyrrole ring (Fig. 3). Interestingly, the unsubstituted **DTP$_1$** compounds do not show the small absorption at about 340 nm like the other members of that family; this is coherent with the less pronounced shoulder in the experimental spectrum evidenced in that region. A comparison of the computed spectra for the **DTP$_1$-Hex** and the **DTP$_2$-Hex** is shown in Fig. 5, where the spectrum has been obtained enveloping each transition with a Gaussian function of fixed half length width of 0.06 eV. One can see that besides some difference in relative intensities the general structure of the spectrum is well reproduced in the higher wavelength region.[45] All the computed transitions for both classes of compounds are of π–π* type as it is confirmed by an excited state analysis. The frontier Kohn–Sham orbitals are reported in Fig. 6 for **DTP$_1$-Hex** and **DTP$_2$-Hex** and although somehow difficult to glance from a simple (delocalized) molecular orbital picture, the more extended nature of the conjugated π system in case of **DTP$_2$** appears to be confirmed.

As shown in Table 2, an irreversible oxidation of the ligands occurs at around 1 V (*vs*. SCE) for the **DTP$_1$** series and at 0.8 V (*vs*. SCE) for the **DTP$_2$** series, respectively. For the same concentration, **DTP$_1$** series exhibited a current twice higher than in the **DTP$_2$** series. Therefore, this irreversible oxidation can be attributed to radical cation formation on the external thiophene. This comparison confirms that the electronic interaction between the **DTP** group and the bipyridine *via* the styryl moiety is higher in the **DTP$_2$** series as described above. In the negative potential

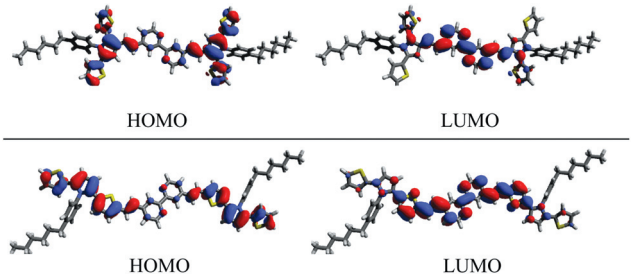

Fig. 6 **DTP$_1$-Hex** (top) and **DTP$_2$-Hex** (bottom) frontier orbitals iso-density contour.

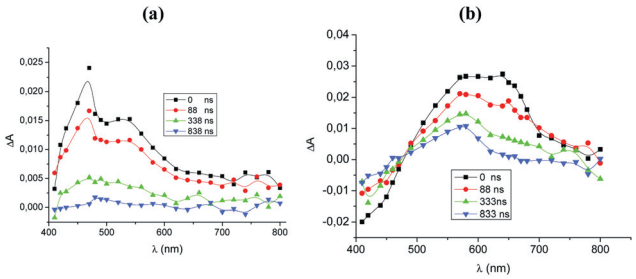

Fig. 7 Transient triplet absorption of **DTP$_1$-F** (a) and **DTP$_2$-F** (b) in DMF (λ_{exc} = 355 nm, 0–838 ns interval). 0 delay corresponds to the initial absorption. The negative signal due to singlet bleaching and to laser induced emission is here excluded.

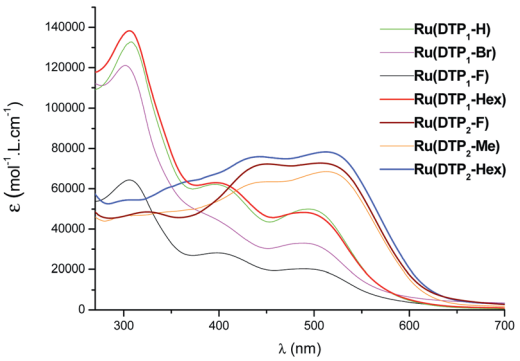

Fig. 8 Absorption spectra of complexes in acetonitrile.

part, the reduction mechanisms of the ligands are also irreversible. They correspond to the addition of an electron in the LUMO, which is centered on the bipyridine group as shown in Fig. 6. In agreement with the electronic interaction, the LUMO potentials are 0.3 V more negative in the **DTP$_1$** series. Due to the pseudo-orthogonality of the dihedral angle between the phenyl ring and the pyrrole group, the donor (methyl, hexyl) or withdrawing (F, Br) effects of the substituent on the phenyl are scarcely significant on the oxidation and reduction potential values. These small effects were also difficult to detect due to the irreversible nature of the electrochemical processes under investigation. All the free ligands were found to be emitting in fluid solution of DMSO (Table 2), DMF and THF (ESI, Tables S1 and S2†) in the nanosecond time scale. However, while a change in the solvent did not cause a notable energy shift of the ground state absorption (ESI, Fig. S2†), it resulted in an evident modification of the emission maxima, which underwent a 30–40 nm blue-shift passing from DMF to THF (ESI, Fig. S2 and S3†), probably due to excited state destabilization in the less polar solvent, suggesting the presence of some degree of charge transfer/separation in the excited state. The emission kinetics were not trivial either, being biexponential for both the **DTP$_1$** and **DTP$_2$** series in DMF (ESI, Tables S1 and S2†). In the **DTP$_2$** series the emission decays became mono-exponential in THF (ESI, Table S1†) and were accompanied by a threefold increase in lifetime (from *ca.* 0.5 to 1.5 ns). In the case of the **DTP$_1$** series, the bi-exponentiality of the decay was maintained also in THF, where two components weighing approximately 50% with a respective lifetime of *ca.* 0.8 and 2 ns were observed. Any attempt to fit the decay with a monoexponential function was, in such cases, a failure, generating unacceptable $\chi^2 > 10$. The **DTP$_1$** behavior was tentatively explained by the presence of two energetically close excited states, both contributing to the broad emission band. Indeed the excitation spectrum showed a dependence upon the observation wavelength, showing two reasonably well resolved bands (323 and 367 nm) (ESI, Fig. S4†) whose relative intensity changed as a function of the observation wavelength. In particular it was observed that the excitation spectrum bore a closer resemblance to the ground state absorption spectrum when the emission was observed at 430 nm (in the blue portion of the emission band), whereas the 367 nm band gradually gained intensity when the observation wavelength was moved to the red. The emission lifetime changed accordingly, undergoing, for example in the case of **DTP$_1$-F**, $a \approx 20\%$ shortening when measured at 430 nm (0.65 ns) with respect to the value obtained in the band maximum (500 nm, 0.84 ns). On the other hand the excitation spectra of the **DTP$_2$** family were generally in good agreement with the ground state absorption (ESI, Fig. S5†).

Upon 355 nm laser excitation the **DTP$_1$** family originated a laser pulse limited negative signal due to ground state bleaching and laser induced emission, followed by a relatively long lived triplet absorption (monoexponential, $\tau \approx 240$ ns) with a distinct 470 nm maximum, followed by a 540 nm shoulder (Fig. 7(a) showing the transient triplet absorption of **DTP$_1$-F**). The **DTP$_2$** ligands were characterized by a relatively weak ground state bleaching in the 400–500 nm interval, followed by an intense and broad absorption (monoexponential $\tau \approx 300$ ns) with a plateau between 550 and 650 nm (Fig. 7(b) showing the transient triplet absorption of **DTP$_2$-F**). The same features were generally found in the transient spectra of the Zn^{2+}–ligand adducts (ESI, Fig. S7 and S8†).[46]

3. Characterization of complexes

The absorption spectra of ruthenium homoleptic complexes, reported in Fig. 8 and Table 3, also reflected the influence of the two ligand families. **Ru(DTP$_1$-X)** complexes showed three absorption bands: a first intense band in the UV region near 300 nm and two others in the visible region near 400 nm and 490 nm. **Ru(DTP$_1$-H)** and **Ru(DTP$_1$-Hex)** bearing respectively a hydrogen and a hexyl group on the phenyl gave similar spectra with comparable ε values. In contrast, when electron withdrawing groups were introduced on the ligand, such as bromine (**Ru(DTP$_1$-Br)**) or fluorine (**Ru(DTP$_1$-F)**), the absorbance was decreased, especially with the latter complex for which half the ε

value was obtained (20 300 L M^{-1} cm^{-1} (490 nm) compared to 50 000 L M^{-1} cm^{-1} (495 nm) for **Ru(DTP$_1$-H)**).

In contrast, the **Ru(DTP$_2$-X)** series exhibited a wide absorption domain in the visible region with λ_{max} at 443–451 and 512–513 nm. In comparison with the **Ru(DTP$_1$-X)** complexes, these bands in the visible region were found to be red-shifted and were found to be of lower intensity in the UV region. The high molar extinction coefficients were almost constant along the visible domain. The electrochemical behavior of the ruthenium complexes was studied by cyclic voltammetry. They show two oxidation waves, the first one is semi-reversible and corresponds to the Ru^{II}–Ru^{III} couple, the second one is irreversible and is attributed to the formation of radical cation on the thiophene as described for the ligands. The first reduction wave corresponds to the transfer of an electron in the bipyridine which is obviously easier in the complexes that in the ligands. The comparison of these potentials confirms the electronic behaviour previously described for the ligands, *i.e.* a higher degree of conjugation in the **DTP$_2$** compared to the **DTP$_1$** series.

The **RuDTP$_1$** series was emitting in fluid solution. When the ligand manifold was excited, two distinct emission bands were observed, one centered in the 480–550 nm region, depending on the ligand, bearing a close similarity in both energy and lifetime with the free ligand fluorescence, and one in the red part of the spectrum (centered around 690 nm) originated by the typical ^{3}MLCT radiative deactivation. Excitation of the lowest energy absorption band (490–505 nm in DMF) resulted only in the low energy emission (ESI, Fig. S10†), whose maximum varied very little within the above mentioned series. The excitation spectrum observed in correspondence of the low energy emission (687–692 nm) was in excellent agreement with the absorption spectrum of the complex, showing three distinct well resolved bands (ESI, Fig. S11†), whereas the excitation spectrum observed in correspondence of the ligand centred (LC) emission revealed two UV bands at 300 and 362 nm, whose shape recalled the absorption features of the Zn^{2+}-**DTP$_1$** adducts (Fig. S6†).

Transient absorption (TA) spectra of the **RuDTP$_1$** complexes in DMF by using a laser excitation at 532 nm (≈10 mJ per pulse) (Fig. 9) exhibited similar characteristics consistent with a long lived triplet MLCT excited state.

An intense absorption was observed in the blue region at 480 nm, followed by an equally intense bleaching of the MLCT band with a minimum centered at 510 nm, followed by a strong featureless triplet absorption in the red part of the visible domain. The excited state lifetime was in the 200–220 ns range for all complexes and the decay was monoexponential. The excited/ground state isosbestic point was found at about 490 nm. By comparison with the TA of the free ligand and of the Zn^{2+} adduct (ESI, Fig. S6 and S8†), the 480 nm band could be assigned to ligand centred LUMO → LUMO + *n* absorption, populated by excitation of the charge transfer band.

Upon 355 nm (mainly ligand absorption manifold) excitation (ESI, Fig. S14†) similar spectra were obtained; however, compared to that observed upon 532 nm excitation, the bleaching of the MLCT band was about half of the intensity of the characteristic 480 nm ligand centred (LC) absorption, the low energy (λ > 600 nm) absorption was flat and about half less intense, both characteristics recalling the spectral features of the parent ligand and of the relative Zn^{2+} adduct and indicating the persistence of the ligand centred excited state and the incomplete relaxation to the MLCT state.

Surprisingly, no MLCT type emission was observed within the **RuDTP$_2$** series, the only emission being that of the LC type in the 512–580 nm region, as confirmed by the similar energy, lifetime and by the excitation spectra obtained in correspondence of the emission maxima (ESI, Fig. S12†). Attempts to detect MLCT emission upon excitation at 532 nm at low temperature (77 K) for **RuDTP$_2$-F** also failed indicating that the non-radiative decay is dominant in the **RuDTP$_2$** series even in a frozen matrix. Interestingly, compared to the parent free ligand, the **RuDTP$_2$-F** emission was substantially blue-shifted (512 *vs.* 570 nm) and its lifetime increased accordingly (from 0.4 to 2 ns), probably due to destabilization caused by strong interaction with the dπ orbital of the metal. The TA spectra obtained following 532 nm excitation (Fig. 10) were generally characterized by

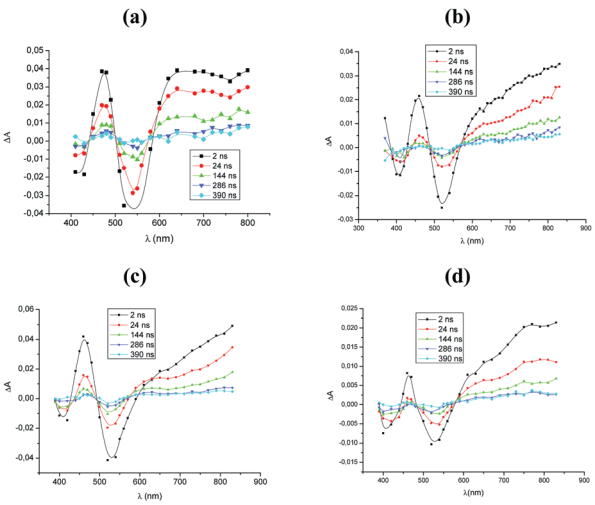

Fig. 9 Transient absorption spectra of **RuDTP$_1$ series** in DMF (λ_{exc} = 532 nm). **RuDTP$_1$-H** (a), **RuDTP$_1$-Br** (b), **RuDTP$_1$-F** (c), **RuDTP$_1$-Hex** (d).

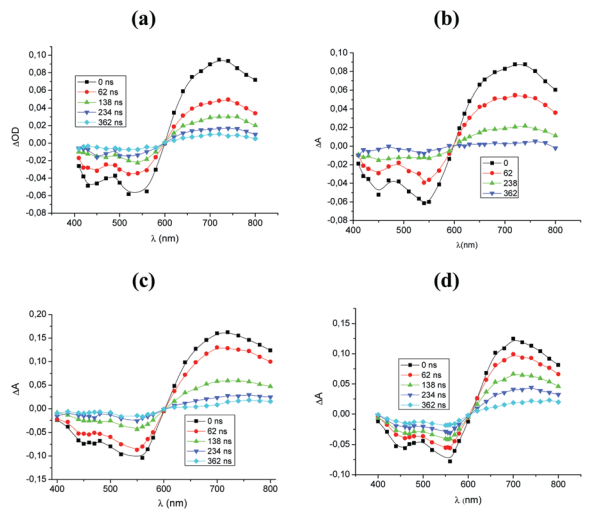

Fig. 10 Transient absorption spectra of **RuDTP$_2$ series** in DMF (λ_{exc} = 532 nm). **RuDTP$_2$-Hex** (a), **RuDTP$_2$-Hex** (b) (λ_{exc} = 355 nm), **RuDTP$_2$-Me** (c), **RuDTP$_2$-F** (d).

a monoexponetial decay, with lifetimes in the 150–200 ns range. All TA spectra shared common features, summarized by the ground state bleaching, which mirrored the two overlapping bands of the ground state absorption, and by the strong triplet–triplet absorption with a maximum at 700 nm. The isosbestic point could be quite accurately individuated at 600 nm. The strong absorption into the red part of the spectrum is evident in the TA of the free ligand and of the Zn^{2+} adduct (ESI, Fig. S7 and S9†), although its maximum was blue-shifted by about 100 nm and probably originates from the LUMO → LUMO + *n* absorption. In this sense, the 100 nm red-shift in the Ru(II) complexes may not be surprising, given that the LUMO π* orbital may be more strongly destabilized upon interaction with the occupied dπ orbitals of the metal resulting in a decreased LUMO–LUMO + *n* energy gap. In this case, the TA spectra collected following 355 nm excitation (Fig. 10(b)) were almost superimposable to those obtained with the 532 nm excitation, suggesting a strong coupling between the metal and the ligand. This fact and the lack of a distinct MLCT emission even upon direct excitation of the lowest energy band (λ > 500 nm) may suggest that the description of the excited state of the **RuDTP$_2$** complexes in terms of usual localized states (hole on the metal, electron on the LUMO orbital of the ligand) may not be entirely appropriate, and, as a result of the strong mixing of the HOMOs of the metal and of the ligand, a photoexcited hole delocalization would result in a favored deactivation of the lowest excited state by internal conversion.

As for the ligands, the homoleptic complexes have been optimized at DFT level with B3LYP functional. Excited states have been computed at TD-DFT level with CAM-B3LYP correlation exchange functional. In that case we used a LANL2DZ[47] basis allowing to treat Ru inner electrons with pseudopotentials. Due to the very high computational cost excited states have been computed using again the relatively small LANL2DZ basis. The latter is certainly not sufficient to provide a qualitative agreement with experimental data, but the main feature of the spectrum can be inferred and the nature of the transition can be easily interpreted. The computed principal transition in the lower energy region of the spectrum can be seen in Table 5 for the two families. Consistent with experimental results the **DTP$_2$** family is significantly red-shifted with respect to the **DTP$_1$** members, the intensities also appear much higher. Note also that the low lying spectrum of the **DTP$_2$** family is composed of a series of transitions all having almost the same intensity, an occurrence that can be related to the extended plateau observed in the experimental spectrum, although in the computed result the low frequency transition appears closer between them than in the experimental one.

The last occurrence, as well as the general blue-shifting of the spectrum can be related to the small basis set used during computation due to the important size of the system. In order to better analyse the excited state's nature we considered natural transition orbitals (NTO)[48,49] representation of the electronic transition. For the reader's convenience we remind that NTOs are obtained by a singular value decomposition (SVD) of the transition density matrix, and they can be considered as the optimal orbitals to represent an electronic transition in the TDDFT formalism. In contrast with Kohn–Sham molecular orbitals base, which require many occupied–virtual orbital couples in NTO base, only one or at maximum two couples entirely describe all the physics underlining the transition. Therefore, "occupied" NTO can be seen as the "hole" orbital, *i.e.* the orbital from which electron is removed during transition, while "virtual" NTO is the orbital in which electron is placed in the excited state.

Table 5 Complexes TDDFT computed principal excitation wavelengths and oscillator strength

X	Ru(DTP$_1$-X) λ^a (nm), (f)	Ru(DTP$_2$-X) λ^a (nm), (f)
H	433.80 (0.99)	498.23 (1.94)
	433.23 (1.02)	496.40 (1.81)
	431.00 (0.70)	490.32 (3.30)
	374.28 (2.42)	487.90 (2.47)
	—	486.57 (1.92)
	—	420.15 (0.50)
Br	433.03 (1.04)	492.86 (2.01)
	432.39 (1.07)	492.15 (1.90)
	430.62 (0.66)	484.81 (3.54)
	371.89 (2.68)	483.02 (2.03)
	—	482.30 (1.78)
	—	419.08 (0.56)
F	432.32 (1.02)	492.09 (1.86)
	431.97 (1.05)	491.50 (2.01)
	429.98 (0.64)	483.75 (3.72)
	371.58 (2.58)	482.19 (1.76)
	—	481.61 (1.89)
	—	419.13 (0.58)
Me	434.03 (0.95)	498.79 (1.81)
	433.49 (1.01)	497.93 (1.98)
	431.12 (0.73)	490.67 (3.86)
	375.31 (1.77)	489.33 (1.82)
	—	488.34 (1.98)
	—	420.64 (0.49)
Hex	433.67 (0.85)	500.40 (1.91)
	433.00 (0.90)	499.12 (1.94)
	430.77 (0.78)	492.24 (3.58)
	375.36 (2.51)	490.57 (1.98)
	—	489.37 (2.05)
	—	422.49 (0.49)

[a] Oscillator strength in parentheses.

NTOs for one of the low lying transitions of the **DTP$_1$-F** and **DTP$_2$-F** are shown in Fig. 11, (note that the other substituents do not qualitatively alter the orbitals). It can be seen easily that although in the two cases the transition are mainly of MLCT nature a significant participation of the ligand in the occupied orbital is observed (especially for **DTP$_2$-F**). This effect can be extremely important in the case of their use as DSSC sensitizers, since such a transition will leave the "hole" far from the semiconductor surface, so diminishing recombination occurrence and facilitating the access of the redox mediator. One can also see that, as expected and consistent with the observed red-shift, the **DTP$_2$-F** shows a larger delocalization of the electronic density in the virtual orbital, leading to a stabilization of the excited state and hence to a red-shift.

Conclusions

A new family of ligands has been obtained by binding bipyridine to dithienylpyrrole (DTP) moieties. To our knowledge, despite interesting electronic properties of DTP, neither DTP-containing bipyridine ligands nor their ruthenium complexes have been reported yet. The electronic properties are deeply modified with

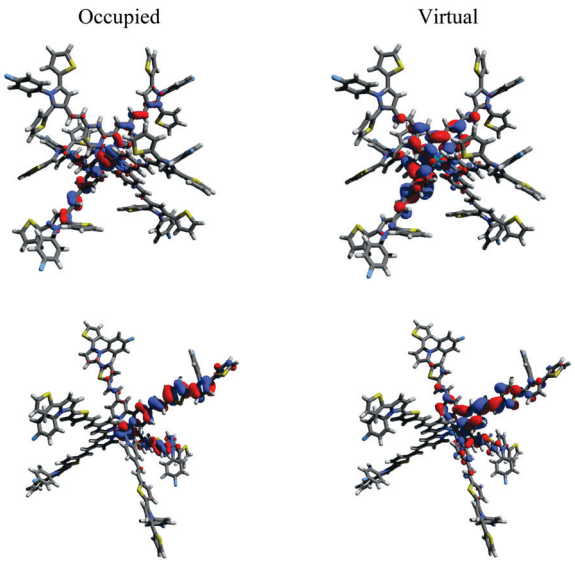

Fig. 11 NTOs isodensity surface: **DTP_1-F** at 432 nm (top) and **DTP_2-F** at 492 nm (bottom). See Table 5 for transitions.

regard to the binding site of bipyridine to DTP. When bound to the pyrrole ring (**DTP_1**), the ligands absorbed the UV part of the spectrum. In this series, substitution of DTP by a fluorine atom induced a huge increase in the absorbance. When bipyridine was bound to the thiophene (**DTP_2**) a strong bathochromic effect was observed leading to a strong absorption in the visible region. The corresponding homoleptic ruthenium complexes exhibited the same features. The complexes from the **DTP_2** series offered a promising absorption range in the visible domain with a notable and constant molar extinction coefficient all along this domain. Calculations as well as transient spectroscopy were used to explain such differences by evidencing a larger π-delocalization extent in **DTP_2** series. In summary, DTP-containing ligands and ruthenium complexes are promising as light harvesters and work is in progress to involve them in photosensitization of semiconductors in dye-sensitized solar cells.

Experimental

Synthesis

All reactions were carried out under an argon atmosphere, whereas workup procedures were done in air. THF and toluene were distilled through MBraun solvent purification system (MB SPS-800) prior to use. *N*,*N*-Dimethylformamide (DMF) was purified by distillation under reduced pressure. Deuterated solvents and commercially available reagents were used as received. Compounds **1–5** [38] and tetraethyl(4,4′-diphosphonate-2,2′-bipyridine)[39] were synthesized by the procedures already reported in literature. Microwave synthesis was performed on CEM Discover device fitted with infrared probe temperature control.

Measurements

^{1}H and ^{13}C NMR spectra were performed on AC200, AC250, or DRX400 Bruker spectrometers at ambient temperature. The chemical shifts (δ), were calibrated by using either tetramethylsilane (TMS) or signals from the residual protons of the deuterated solvents, and are reported in parts per million (ppm) from low- to high-field. Standard abbreviations indicating multiplicity are used as follows: s = singlet; d = doublet; t = triplet; m = multiplet; dd = doublet of doublets. All coupling constants are reported in Hz. High-resolution mass spectrometry (HRMS) data were obtained by using a Bruker micrOTOF-Q spectrometer. UV-vis spectra were recorded in a 1 cm path length quartz cell on a LAMBDA 1050 (Perkin Elmer), spectrophotometer. Emission and excitation spectra were obtained on optically diluted solutions by using a Fluoromax 2 (Jobin Yvon) Spectrofluorometer.

Cyclic voltammetry was performed on a Radiometer PST006 potentiostat using a conventional three-electrode cell. The potassium chloride saturated calomel electrode (SCE) was separated from the test compartment using a bridge tube. The test solution was DMF containing 0.1 M tetrabutylammonium hexafluorophosphate as supporting electrolyte. The working electrode was a 10 mm Pt wire and the counter-electrode a 1 cm^2 vitreous carbon disc. The solutions were purged with argon before each measurement.

A 0.5 mM solution of the studied compound was generally used. All potentials were quoted *versus* SCE. In these conditions the redox potential of the couple Fc^+–Fc was found at 0.47 V. In all the experiments the scan rate was 100 mV s^{-1}.

Singlet emission lifetimes were acquired by using a Picoharp 300 time correlated single photon counting (TCSPC) apparatus by using the 380 nm excitation generated by a nano-led with a repetition rate of 10 MHz. The maximum reliable time resolution of the apparatus was 300 ps. The average number of fluorescence counts per seconds (cps) in optically diluted solutions ($A_{380} \approx 0.2$) were in the range 10^3–10^4. The emission decay was deconvolved and statistically elaborated by means of the Fluofit® dedicated program. The fitting was deemed satisfactory when $0.99 < \chi^2 < 1.02$ and the residues were homogeneously distributed around 0 along the whole time interval under consideration (typically 20 ns). In the case of multiexponential decay, the amplitude weighted average lifetime was considered.

Transient absorption spectroscopy experiments were carried out by using a previously described nanosecond transient absorption apparatus.[50] If necessary, in the case of weak signals (ligand based triplet absorption), to obtain a satisfactory S/N ratio, oscillographic traces were averaged over 5–10 laser shots.

Computations

All quantum chemistry calculations have been performed using GAUSSIAN 09 suite of codes.[51] In the case of the ligands geometry optimization has been done by using 6-31G basis set and B3LYP exchange correlation functional. Subsequently UV-vis spectrum has been simulated computing 25 excited states at TD-DFT level using CAM-B3LYP functional and 6-31G+(d,p) basis set. In the case of the complexes geometry optimization was performed using LANL2DZ basis and B3LYP functional, again 25 excited states have been computed using the same LANL2DZ basis and CAM-B3LYP functional. Excited states analysis in terms of NTOs have been performed using a local produced and free downloadable code NancyEX (see http://www.nancyex.sourceforge.net/).

Synthesis of ligands

General procedure for synthesis of aldehydes 6–8. In a round bottomed flask, phosphorus oxychloride (6 mmol, 0.55 mL) was added to DMF (12 mL) at 0 °C and the mixture was stirred for 15 minutes. **2**, **3** or **4** (1.5 mmol) was dissolved in 5 mL of DMF and added to the previous solution over a period of 30 minutes at 0 °C. The resulting red coloured mixture was stirred overnight and then heated at 70 °C for 1 h. The reaction mixture was then cooled and poured into ice. The yellow precipitates were formed that were filtered and dried. The crude product was purified by column chromatography on silica gel.

6: Yellow solid, yield: 50%. Eluent: cyclohexane : ethyl acetate (4 : 1). ^{1}H NMR (250 MHz, $CDCl_3$), δ (ppm): 9.90 (s, 1H), 7.51 (dd, J = 8.7 and 2.8 Hz, 2H), 7.38 (dd, J = 5.0 and 1.3 Hz, 1H), 7.19 (dd, J = 5.2 and 1.1 Hz, 1H), 7.09 (dd, J = 8.6 and 2.8 Hz, 2H), 7.02 (s, 1H), 6.97 (m, 2H), 6.89 (dd, J = 5.1 and 3.7 Hz, 1H), 6.64 (dd, J = 3.7 and 1.1 Hz, 1H). ^{13}C NMR (62.5 MHz, $CDCl_3$), δ (ppm): 186.5, 132.9, 131.6, 131.4, 129.4, 127.7, 127.6, 126.9, 126.4, 125.5, 108.5.

7: Yellow solid, yield: 65%. Eluent: cyclohexane : ethyl acetate (2 : 1). ^{1}H NMR (250 MHz, $CDCl_3$), δ (ppm): 9.91 (s, 1H), 7.36 (dd, J = 4.5 and 1.8 Hz, 1H), 7.21 (dd, J = 2.8 and 1.8 Hz, 1H), 7.18 (dd, J = 3.5 and 2.2 Hz, 2H), 7.08 (dd, J = 3.5 and 2.2 Hz, 2H), 7.05 (s, 1H), 6.98 (m, 2H), 6.88 (dd, J = 5.1 and 3.6 Hz, 1H), 6.65 (dd, J = 3.6 and 1.1 Hz, 1H). ^{13}C NMR (62.5 MHz, $CDCl_3$), δ (ppm): 188.3, 166.1, 162.0, 138.3, 133.0, 131.6, 131.4, 131.3, 131.1, 129.2, 129.0, 127.3, 127.1, 126.4, 125.6, 126.0, 125.3.

8: Yellow solid, yield: 60%. Eluent: cyclohexane : ethyl acetate (2 : 1). ^{1}H NMR (250 MHz, $CDCl_3$), δ (ppm): 9.92 (s, 1H), 7.33 (dd, J = 3.5 and 0.7 Hz, 1H), 7.16 (m, 5H), 7.06 (s, 1H), 6.96 (m, 2H), 6.84 (dd, J = 5.0 and 1.2 Hz, 1H), 6.61 (dd, J = 3.5 and 2.7 Hz, 1H), 2.69 (t, J = 7.6 Hz, 2H), 1.63 (m, 2H), 1.35 (m, 6H), 0.93 (m, 3H). ^{13}C NMR (62.5 MHz, $CDCl_3$), δ (ppm): 186.8, 131.7, 131.0, 129.3, 128.7, 127.2, 127.0, 126.0, 125.6, 125.1, 107.7, 36.0, 32.1, 31.5, 29.2, 23.1, 14.6.

9a: **6** (1 mmol, 414 mg), ethylene glycol (6 mmol, 0.33 mL) and *p*-toluenesulfonic acid (0.025 mmol, 4.75 mg) were dissolved in 30 mL of toluene. The reaction mixture was refluxed for 16 h under Dean–Stark conditions and then washed three times with 1% aqueous NaOH solution and water respectively. The organic phase was dried over anhydrous $MgSO_4$, filtered and evaporated under vacuum to afford **9a**, yield: 94%. ^{1}H NMR (250 MHz, $CDCl_3$), δ (ppm): 7.44 (d, J = 8.6 Hz, 2H), 7.25 (dd, J = 4.1 and 1.9 Hz, 1H), 7.11 (dd, J = 5.9 and 1.0 Hz, 1H), 7.05 (d, J = 8.6 Hz, 2H), 6.93 (m, 2H), 6.85 (dd, J = 5.1 and 3.6 Hz, 1H), 6.71 (s, 1H), 6.57 (dd, J = 3.6 and 1.0, 1H), 5.78 (s, 1H), 4.21 (m, 2H), 4.01 (m, 2H).

9: **9a** (0.80 mmol, 370 mg) was dissolved in 12 mL of THF. To this solution *n*-BuLi (1.5 M solution in hexanes) (0.96 mmol, 0.64 mL) was added dropwise at −40 °C. Reaction progress was monitored by TLC, after completion of metallation (about 2 hours) the reaction mixture was hydrolyzed by adding water and extracted with CH_2Cl_2 and the separated organic layer was washed with water, dried over $MgSO_4$ and evaporated under vacuum to afford a green product that was subjected to the next step without purification. The above obtained product (0.66 mmol, 250 mg), 10 mL water and *p*-toluenesulfonic acid (0.79 mmol, 150.6 mg) were dissolved in 25 mL of acetone. Then 0.06 mL of 4-picoline was added and the reaction mixture was refluxed for 24 h. Then it was cooled and extracted with CH_2Cl_2 and washed with saturated aqueous $NaHCO_3$ and water, dried over $MgSO_4$, concentrated *in vacuo* and purified by column chromatography on silica gel (eluent: cyclohexane : ethyl acetate 4 : 1) to afford green powdered product, yield: 81%. ^{1}H NMR (250 MHz, $CDCl_3$), δ (ppm): 9.90 (s, 1H), 7.39 (m, 3H), 7.34 (d, J = 3.3 Hz, 1H), 7.22 (d, J = 7.0 Hz, 2H), 7.14 (d, J = 5.0 Hz, 1H), 7.04 (s, 1H), 6.96 (d, J = 3.1 Hz, 2H), 6.85 (t, J = 3.8 Hz, 1H), 6.61 (d, J = 3.34 Hz, 1H). ^{13}C NMR (62.5 MHz, $CDCl_3$), δ (ppm): 186.6, 137.4, 137.2, 133.4, 131.7, 131.0, 129.6, 129.2, 128.8, 127.2, 127.0, 126.2, 125.7, 125.2, 108.0.

General procedure for preparation of 10a, 11a, 12a. **3**, **4** or **5** (6.14 mmol) was dissolved in a mixture of 90 mL chloroform and 9 mL of propanoic acid at −50 °C. To this solution *N*-bromosuccinimide (6.45 mmol, 1.15 mg) was added. The reaction mixture was stirred at this temperature for 1.5 hours. After that, the reaction was quenched by adding water. The reaction mixture was washed with 1% aqueous NaOH solution and water and then dried over anhydrous $MgSO_4$. Solvent was evaporated and the crude product was used as such for next step without any purification.

General procedure for preparation of 10, 11, 12. **10a**, **11a** or **12a** (2 mmol) was dissolved in 25 mL of THF. To this solution n-BuLi (1.6 M solution in hexanes; 3 mmol, 1.87 mL) was added dropwise at −40 °C. Reaction progress was monitored by TLC, after completion of metallation (about 1.5 h) the temperature was decreased at −78 °C and a THF solution of DMF (8 mmol, 0.56 mL) was added dropwise. Temperature was slowly raised to room temperature. The reaction mixture was stirred overnight and quenched by adding water. After extraction with CH_2Cl_2, the separated organic layer was washed with water and dried over $MgSO_4$. The crude product was purified by column chromatography on silica gel.

10: Yellow solid, yield: 45%. Eluent: ethyl acetate : cyclohexane (1 : 4). ^{1}H NMR (200 MHz, $CDCl_3$), δ (ppm): 9.86 (s, 1H), 7.57 (d, J = 4.0 Hz, 1H), 7.40 (d, J = 8.6 Hz, 2H), 7.34 (d, J = 8.6 Hz, 2H), 7.21 (dd, J = 5.2 and 0.9 Hz, 1H), 6.94 (dd, J = 4.8 and 3.7 Hz, 1H), 6.86 (d, J = 4.0 Hz, 1H), 6.78 (d, J = 4.0 Hz, 1H), 6.71 (dd, J = 2.5 and 1.0 Hz, 1H), 6.68 (d, J = 3.9 Hz, 1H). ^{13}C NMR (62.5 MHz, $CDCl_3$), δ (ppm): 182.4, 144.9, 140.9, 136.9, 133.9, 133.1, 132.0, 129.6, 127.4, 125.4, 123.3, 117.6, 117.0, 112.8, 111.1.

11: Dark orange oil, yield: 55%. Eluent: ethyl acetate : cyclohexane (1 : 4). ^{1}H NMR (250 MHz, $CDCl_3$), δ (ppm): 9.69 (s, 1H), 7.44 (d, J = 4.1 Hz, 1H), 7.25 (m, 4H), 7.09 (dd, J = 5.1 and 1.1 Hz, 1H), 6.83 (dd, J = 5.1 and 3.7 Hz, 1H), 6.77 (d, J = 4.0 Hz, 1H), 6.66 (d, J = 4.1 Hz, 1H), 6.59 (m, 2H), 2.51 (s, 3H). ^{13}C NMR (62.5 MHz, $CDCl_3$), δ (ppm): 182.3, 145.7, 140.7, 137.3, 135.4, 133.2, 130.9, 130.1, 129.6, 127.4, 125.1, 124.2, 112.7, 110.8, 21.8.

12: Green oil, yield: 43%. Eluent: ethyl acetate : cyclohexane 1 : 4). ^{1}H NMR (250 MHz, $CDCl_3$), δ (ppm): 9.75 (s, 1H), 7.43 (d, J = 4.1 Hz, 1H), 7.26 (m, 4H), 7.07 (d, J = 5.1 Hz, 1H), 6.81 (dd, J = 5.0 and 3.7 Hz, 1H), 6.76 (d, J = 4.0 Hz, 1H), 6.60 (m, 3 H), 2.72 (t, J = 7.4 Hz, 2H), 1.69 (m, 2H), 1.34 (m, 6H), 0.92

(t, J = 6.7 Hz, 3H). ^{13}C NMR (62.5 MHz, $CDCl_3$), δ (ppm): 182.78, 145.78, 140.85, 137.26, 135.68, 134.79, 133.37, 130.37, 129.95, 127.72, 125.33, 124.38, 112.82, 110.95, 36.37, 32.35, 31.94, 29.46, 23.29, 14.84.

General procedure for synthesis of ligands from aldehydes 6–12. The aldehyde (0.43 mmol, 145 mg) and tetraethyl(4,4′-diphosphonate-2,2′-bipyridine) (0.216 mmol, 98.4 mg) were dissolved in 10 mL of deoxygenated anhydrous THF. Solid potassium *tert*-butoxide (0.64 mmol, 71.8 mg) was added rapidly. The resulting solution was stirred at room temperature overnight. Afterwards, methanol was added to the reaction mixture, brown precipitates were formed that were filtered and washed with an excess of methanol.

DTP$_1$-H: Starting from **9**, yellow solid, yield: 68%. ^{1}H NMR (250 MHz, DMSO-d_6), δ (ppm): 8.64 (d, J = 4.8 Hz, 2H), 8.43 (s, 2H), 7.63 (d, J = 4.5 Hz, 2H), 7.54 (m, 12H), 6.32 (m, 6H), 7.19 (s, 2H), 7.10 (t, J = 3.4 Hz, 2H), 6.97 (m, 4H), 6.74 (d, J = 2.7 Hz, 2H). ^{13}C NMR (62.5 MHz, DMSO-d_6), δ (ppm): 155.8, 149.8, 146.1, 137.3, 133.4, 130.8, 130.4, 129.9, 129.4, 128.5, 127.3, 127.0, 125.9, 125.4, 124.2, 121.9, 120.5, 117.1, 106.6. HRMS calcd for $C_{50}H_{34}N_4S_4$ [M + H]$^+$: 819.1666. Found: 819.1734. Anal. Calcd for $C_{50}H_{34}N_4S_4$: C, 73.32; H, 4.18; N, 6.84; S, 15.66%. Found: C, 72.95; H, 4.17; N, 6.54; S, 15.31%. UV-vis (DMSO), λ_{max} (nm) (ε (10^3 M^{-1} cm^{-1})) = 311 (53.9) and 352 (42.1).

DTP$_1$-Br: Starting from **6**, yellow solid, yield: 38%. ^{1}H NMR (400 MHz, $CDCl_3$), δ (ppm): 8.58 (d, J = 5.1 Hz, 2H), 8.35 (s, 2H), 7.46 (dd, J = 8.6 and 1.8 Hz, 4H), 7.42 (d, J = 16.1, 2H), 7.33 (m, 4H), 7.18 (dd, J = 5.1 and 1.0 Hz, 2H), 7.07 (dd, J = 8.6 and 1.9 Hz, 4H), 7.0 (m, 4H), 6.90 (dd, J = 5.1 and 1.4 Hz, 2H), 6.87 (s, 2H), 6.85 (dd, J = 3.5 and 1.0 Hz, 2H), 6.61 (dd, J = 3.6 and 1.0 Hz, 2H). ^{13}C NMR (100 MHz, $CDCl_3$), 157.2, 149.7, 146.9, 137.4, 134.2, 132.3, 131.5, 131.2, 131.0, 130.7, 129.8, 129.4, 129.0, 127.8, 127.3, 127.1, 125.8, 125.3, 124.5, 122.9, 120.3, 118.7, 107.0. HRMS calcd for $C_{50}H_{32}Br_2N_4S_4$ [M + H]$^+$: 974.9873. Found: = 974.9933. Anal. Calcd for $C_{50}H_{32}Br_2N_4S_4$: C, 61.48; H, 3.30; N, 5.73; S, 13.13%. Found: C, 61.16; H, 3.47; N, 5.42; S, 12.76%. UV-vis (DMSO), λ_{max} (nm) (ε (10^3 M^{-1} cm^{-1})) = 309 (61.0) and 356 (42.4).

DTP$_1$-F: Starting from **7**, yellow solid, yield: 31%. ^{1}H NMR (250 MHz, $CDCl_3$), δ (ppm): 8.60 (d, J = 5.3 Hz, 2H), 8.45 (s, 2H), 7.39 (d, J = 16.1 Hz, 2H), 7.33 (dd, J = 4.1 and 1.0 Hz, 2H), 7.19 (m, 8H), 7.03 (m, 10H), 6.89 (m, 4H), 6.64 (dd, J = 2.6 and 1.0 Hz, 2H). ^{13}C NMR (62.5 MHz, $CDCl_3$), δ (ppm): 165.0, 161.1, 149.0, 133.9, 133.8, 133.8, 131.4, 131.3, 131.0, 130.1, 129.9, 127.7, 127.2, 127.1, 125.7, 125.4, 124.0, 122.6, 120.5, 119.3, 116.4, 116.1, 106.8. HMRS calcd for $C_{50}H_{32}F_2N_4S_4$ [M + H]$^+$: 855.1478. Found: 855.1551. Anal. Calcd for $C_{50}H_{32}F_2N_4S_4$: C, 70.23; H, 3.77; N, 6.55; S, 15.00%. Found: C, 69.92; H, 3.96; N, 6.85; S, 15.06%. UV-vis (DMSO), λ_{max} (nm) (ε (10^3 M^{-1} cm^{-1})) = 309 (52.5) and 360 (39.0).

DTP$_1$-Hex: Starting from **8**, yellow solid, yield: 36%, ^{1}H NMR (400 MHz, $CDCl_3$), δ (ppm): 8.60 (d, J = 5.0Hz, 2H), 8.38 (s, 2H), 7.35 (d, J = 16.1 Hz, 2H), 7.30 (d, J = 5.1 Hz, 2H), 7.15 (m, 12H), 6.98 (m, 4H), 6.93 (s, 2H), 6.86 (t, J = 4.1 Hz, 4H), 6.61 (dd, J = 2.6 and 0.9 Hz, 2H), 2.67 (t, J = 7.6 Hz, 4H), 1.63 (m, 4H), 1.31 (m, 12H), 0.90 (m, 6H). ^{13}C NMR (62.5 MHz, $CDCl_3$), 157.1, 149.8, 147.1, 144.3, 135.8, 134.8, 131.3, 130.9, 129.5, 129.1, 127.4, 127.2, 126.9, 126.2, 125.2, 124.8, 124.1, 122.3, 120.2, 118.7, 106.4, 35.9, 32.1, 31.51, 29.1, 23.0, 14.5. HRMS calcd for $C_{62}H_{58}N_4S_4$ [M + H]$^+$: 987.3617. Found: 987.3544. Anal. Calcd for $C_{62}H_{58}N_4S_4$: C, 75.41; H, 5.92; N, 5.67; S, 12.99%. Found: C, 75.14; H, 5.53; N, 5.59; S, 12.64%. UV-vis (DMSO), λ_{max} (nm) (ε (10^3 M^{-1} cm^{-1})) = 304 (41.6) and 381 (26.0).

DTP$_2$-F: Starting from **10**, light brown solid, yield: 73%. Due to poor solubility in organic solvents, NMR spectra could not be obtained. HRMS calcd for $C_{50}H_{32}F_2N_4S_4$ [M + H]$^+$: 855.1478. Found: 855.1551. Anal. Calcd for $C_{50}H_{32}F_2N_4S_4$: C, 70.23; H, 3.77; N, 6.55; S, 15.00%. Found: C, 69.96; H, 3.74; N, 6.36; S, 14.94%. UV-vis (DMSO), λ_{max} (nm) (ε (10^3 M^{-1} cm^{-1})) = 316 (24.9) and 433 (59.5).

DTP$_2$-Me: Starting from **11**, light brown solid, yield: 46%. Due to poor solubility in organic solvents, NMR spectra could not be obtained. HRMS calcd for $C_{52}H_{38}N_4S_4$ [M + H]$^+$: 847.1979. Found: 847.2052. Anal. Calcd for $C_{52}H_{38}N_4S_4$: C, 73.72; H, 4.52; N, 6.61; S, 15.14%. Found: C, 73.34; H, 4.53; N, 6.43; S, 15.01%. UV-vis (DMSO), λ_{max} (nm) (ε (10^3 M^{-1} cm^{-1})) = 318 (19.1) and 435 (48.2).

DTP$_2$-Hex: Starting from **12**, light brown solid, yield: 40%. ^{1}H NMR (400 MHz, $CDCl_3$), δ (ppm): 8.59 (d, J = 5.1 Hz, 2H), 8.43 (s, 2H), 7.42 (d, J = 16.0 Hz, 2H), 7.27 (m, 12H), 7.05 (dd, J = 5.0 and 0.7 Hz, 2H), 6.85 (d, J = 3.84 Hz, 2H), 6.82 (dd, J = 4.9 and 3.7 Hz, 2 H), 6.71 (d, J = 16.0 Hz, 2H), 6.62 (d, J = 3.8 Hz, 2H), 6.56 (dd, J = 6.6 and 3.8 Hz, 2H), 6.39 (d, J = 3.8 Hz, 2H), 2.75 (t, J = 7.5 Hz, 4H), 1.71 (m, 4H), 1.35 (m, 12H), 0.91 (t, J = 6.7 Hz, 6H). ^{13}C NMR (100 MHz, $CDCl_3$), δ (ppm): 156.89, 149.95, 146.11, 145.15, 139.96, 136.46, 136.21, 135.14, 131.40, 130.31, 129.95, 129.71, 128.71, 127.18, 126.57, 124.63, 124.42, 124.20, 120.86, 117.78, 110.42, 110.05, 36.14, 32.14, 31.67, 29.22, 23.08, 14.56. HRMS calcd for $C_{62}H_{58}N_4S_4$ [M + H]$^+$: 987.3617. Found: 987.3614. Anal. Calcd for $C_{62}H_{58}N_4S_4$: C, 75.41; H, 5.92; N, 5.67; S, 12.99%. Found: C, 75.14; H, 5.62; N, 5.46; S, 12.61%. UV-vis (DMSO), λ_{max} (nm) (ε (10^3 M^{-1} cm^{-1})) = 323 (27.5) and 439 (56.1).

Synthesis of complexes

3 equiv. of ligand and 1 equiv. of $RuCl_2(DMSO)_4$ were suspended into 10 mL of ethylene glycol (see product details for exact amounts). The mixture was irradiated in the microwave oven (250 W, 200 °C, 10 min). On cooling, the red solution was poured into a saturated aqueous solution of KPF_6. A few drops of acetone were also added and left at room temperature overnight. Complex was obtained as red solid that was filtered and washed with water and diethyl ether.

Ru(DTP$_1$-H): Dark red solid, yield: 76%. ^{1}H NMR (400 MHz, DMF-d_7), δ (ppm): 9.03 (s, 6H), 7.92 (d, J = 5.9 Hz, 6H), 7.69 (m, 12H), 7.50 (m, 24H), 7.38 (d, J = 6.7 Hz 12H), 7.25 (d, J = 15.9 Hz, 6H), 7.12 (s, 6H), 7.03 (m, 12H), 6.97 (t, J = 4.5 Hz, 6H), 6.75 (d, J = 2.8 Hz, 6H). HRMS (ESI): calcd for $C_{150}H_{102}N_{12}RuS_{12}$ m/z = 1278.2016 [M − 2PF_6]$^{2+}$. Found: 1278.1987. UV-vis (CH_3CN), λ_{max} (nm) (ε (10^3 M^{-1} cm^{-1})) = 308 (132.8), 396 (62.2) and 495 (50.0).

Ru(DTP$_1$-Br): Dark red solid, yield: 79%. ^{1}H NMR (400 MHz, CD_3CN), δ (ppm): 8.43 (s, 6H), 7.56 (m, 24H), 7.46 (m, 12H), 7.32 (m, 12H), 7.19 (d, J = 8.2 Hz, 12H), 7.10 (d, J =

16.5 Hz, 6H), 7.01 (s, 6H), 6.93 (m, 12H), 6.74 (d, J = 2.6 Hz, 6H). HRMS (ESI): calcd for $C_{150}H_{96}Br_6N_{12}RuS_{12}$ m/z = 1515.9319 $[M - 2PF_6]^{2+}$. Found: 1515.9256. UV-vis (CH_3CN), λ_{max} (nm) (ε (10^3 M^{-1} cm^{-1})) = 264 (112.5), 390 (46.6) and 488 (33.1).

Ru(DTP$_1$-F): Dark red solid, yield: 75%. ^{1}H NMR (400 MHz, DMF-d_7), δ (ppm): 9.06 (s, 6H), 7.93 (d, J = 6.0 Hz, 6H), 7.69 (m, 12H), 7.48 (m, 24H), 7.35 (t, J = 8.4 Hz, 12H), 7.20 (d, J = 16.0 Hz, 6H), 7.14 (s, 6H), 7.08 (m, 12H), 7.03 (dd, J = 5.1 and 1.4 Hz, 6H), 6.85 (d, J = 3.6 Hz, 6H). HRMS (ESI): calcd for $C_{150}H_{96}F_6N_{12}RuS_{12}$ m/z = 1332.1751 $[M - 2PF_6]^{2+}$. Found: 1332.1518. UV-vis (CH_3CN), λ_{max} (nm) (ε (10^3 M^{-1} cm^{-1})) = 306 (64.4), 398 (28.2) and 490 (20.3).

Ru(DTP$_1$-Hex): Dark red solid, yield: 63%. ^{1}H NMR (400 MHz, DMF-d_7), δ (ppm): 9.20 (s, 6H), 8.09 (d, J = 6 Hz, 6H), 7.82 (m, 12H), 7.62 (d, J = 4.8 Hz, 6H), 7.48 (m, 36H), 7.28 (s, 6H), 7.20 (m, 12H), 7.13 (t, J = 4.8 Hz, 6H), 6.93 (d, J = 3.1 Hz, 6H), 2.85 (t, J = 7.0 Hz, 12H), 1.78 (m, 12H), 1.46 (m, 36H), 1.04 (m, 18H). HRMS (ESI): calcd for $C_{186}H_{174}N_{12}RuS_{12}$ m/z = 1530.4833 $[M - 2PF_6]^{2+}$. Found: 1530.4938. UV-vis (CH_3CN), λ_{max} (nm) (ε (10^3 M^{-1} cm^{-1})) = 306 (48.3), 397 (63.1) and 489 (48.3).

Ru(DTP$_2$-F): To remove unreacted ligand resultant product was dissolved in acetone. Complex was soluble whereas ligand remained insoluble. The solution was filtered and complex was again precipitated with saturated aqueous solution of KPF_6. Dark red precipitate was obtained and was filtered and washed with water and diethyl ether, yield: 65%. ^{1}H NMR (400 MHz, DMF-d_7), δ (ppm): 9.25 (s, 6H), 8.15 (m, 12H), 7.82 (m, 12H), 7.65 (t, J = 7.4 Hz, 12H), 7.58 (d, J = 4.7 Hz, 12H), 7.38 (d, J = 2.9 Hz, 6H), 7.15 (m, 12H), 7.00 (dd, J = 8.0 and 3.7 Hz, 12H), 6.92 (dd, J = 8.1 and 3.6 Hz, 12H). HRMS (ESI): calcd for $C_{150}H_{96}F_6N_{12}RuS_{12}$ m/z = 1332.1751 $[M - 2PF_6]^{2+}$. Found: 1332.1698. UV-vis (CH_3CN), λ_{max} (nm) (ε (10^3 M^{-1} cm^{-1})) = 452 (72.3) and 508 (72.7).

Ru(DTP$_2$-Me): Unreacted ligand was removed by following the same method as for **Ru(DTP$_2$-F)**. Dark red solid was obtained, yield: 40%. ^{1}H NMR (400 MHz, DMF-d_7), δ (ppm): 9.07 (s, 6H), 8.01 (m, 12H), 7.64 (m, 6H), 7.38 (m, 30H), 7.15 (d, J = 3.8 Hz, 6H), 6.92 (m, 6H), 6.86 (d, J = 15.5 Hz, 6H), 6.76 (m; 12H), 6.69 (d, J = 3.3 Hz, 6H), 6.63 (d, J = 3.3 Hz, 6H), 2.46 (s, 18H). HRMS (ESI): calcd for $C_{156}H_{114}N_{12}RuS_{12}$ m/z = 1320.2502 $[M - 2PF_6]^{2+}$. Found: 1320.2426. UV-vis (CH_3CN), λ_{max} (nm) (ε (10^3 M^{-1} cm^{-1})) = 451 (62.5) and 512 (67.9).

Ru(DTP$_2$-Hex): Dark red solid, yield: 66%. ^{1}H NMR (400 MHz, DMF-d_7), δ (ppm): 9.12 (s, 6H), 7.95 (m, 12H), 7.66 (d, J = 5.9 Hz, 6H), 7.44 (m, 30H), 7.15 (d, J = 3.7 Hz, 6H), 6.90 (t, J = 4.7 Hz, 6H), 6.85 (d, J = 15.8 Hz, 6H), 6.80 (m, 12H), 6.73 (d, J = 3.7 Hz, 6H), 6.70 (d, J = 3.7 Hz, 6H), 2.75 (m, 12H), 1.71 (m, 12H), 1.27 (m, 36H), 0.77 (t, J = 6.4 Hz, 18H). HRMS (ESI): calcd for $C_{186}H_{174}N_{12}RuS_{12}$ m/z = 1530.4833 $[M - 2PF_6]^{2+}$. Found: 1530.4808. UV-vis (CH_3CN), λ_{max} (nm) (ε (10^3 M^{-1} cm^{-1})) = 360 (62.7), 443 (75.9) and 513 (78.3).

Acknowledgements

The authors would like to thank Brigitte Fernette (NMR), Stéphane Parant (UV-vis) and François Dupire (Mass) for their helpful measurements. Funding from PRIN 2008 (UNIFE) is also gratefully acknowledged.

Notes and references

1 A. Juris, V. Balzani, F. Barigelletti, S. Campagna, P. Belser and A. V. Zelewsky, *Coord. Chem. Rev.*, 1988, **84**, 85–277.
2 A. Juris, S. Campagna, V. Balzani, G. Gremaud and A. V. Zelewsky, *Inorg. Chem.*, 1988, **27**, 3652–3655.
3 J. R. Schoonover, C. A. Bignozzi and T. J. Meyer, *Coord. Chem. Rev.*, 1997, **165**, 239–266.
4 V. Balzani and A. Juris, *Coord. Chem. Rev.*, 2001, **211**, 97–115.
5 B. O'Regan and M. Grätzel, *Nature*, 1991, **353**, 737–740.
6 A. Hagfeldt and M. Grätzel, *Chem. Rev.*, 1995, **95**, 49–68.
7 R. Argazzi, C. A. Bignozzi, G. M. Hasselmann and G. J. Meyer, *Inorg. Chem.*, 1998, **27**, 4533–4537.
8 N. Robertson, *Angew. Chem., Int. Ed.*, 2006, **45**, 2338–2345.
9 J. Otsuki, K. Sato, M. Tsujino, N. Okuda, K. Araki and M. Seno, *Chem. Lett.*, 1996, **10**, 847–848.
10 H. F. M. Nelissen, A. F. J. Schut, F. Venema, M. C. Feiters and R. J. M. Nolte, *Chem. Commun.*, 2000, 577–578.
11 P. Mobian, J.-M. Kern and J.-P. Sauvage, *Angew. Chem., Int. Ed.*, 2004, **43**, 2392–2395.
12 J.-P. Sauvage, *Chem. Commun.*, 2005, 1507–1510.
13 A. Credi, *Aust. J. Chem.*, 2006, **59**, 157–169.
14 S. A. Haque, S. Handa, K. Peter, E. Palomares, M. Thelakkat and J. R. Durrant, *Angew. Chem., Int. Ed.*, 2005, **44**, 5740–5744.
15 S. Ito, N.-L. C. Ha, G. Rothenberger, P. Liska, P. Comte, S. M. Zakeeruddin, P. Pechy, M. K. Nazeeruddin and M. Gratzel, *Chem. Commun.*, 2006, 4004–4006.
16 G. P. Smestad and C. M. Lampert, *Sol. Energy Mater. Sol. Cells*, 2007, **91**, 440–444.
17 D. Martineau, M. Beley, P. C. Gros, S. Cazzanti, S. Caramori and C. A. Bignozzi, *Inorg. Chem.*, 2007, **46**, 2272–2277.
18 A. Grabulosa, D. Martineau, M. Beley, P. C. Gros, S. Cazzanti, S. Caramori and C. A. Bignozzi, *Dalton Trans.*, 2009, 63–70.
19 A. Grabulosa, M. Beley, P. C. Gros, S. Cazzanti, S. Caramori and C. A. Bignozzi, *Inorg. Chem.*, 2009, **48**, 8030–8036.
20 M. Fujii, T. Nishinaga and M. Iyoda, *Tetrahedron Lett.*, 2009, **50**, 555–558.
21 M. M. Oliva, T. M. Pappenfus, J. H. Melby, K. M. Schwaderer, J. C. Johnson, K. A. McGee, D. A. da Silva Filho, J.-L. Bredas, J. Casado and J. T. Lopez Navarrete, *Chem.–Eur. J.*, 2010, **16**, 6866–6876.
22 G. Zotti, S. Martina, G. Wegner and A. D. Schlüter, *Adv. Mater.*, 1992, **4**, 798–801.
23 R. E. Niziurski-Mann, C. Scordilis-Kelley, T. L. Liu, M. P. Cava and R. T. Carlin, *J. Am. Chem. Soc.*, 1993, **115**, 887–891.
24 P. Audebert, S. Sadki, F. Miomandre, P. Hapiot and K. Chane-Ching, *New J. Chem.*, 2003, **27**, 798–804.
25 T. M. Pappenfus, B. J. Hermanson, T. J. Helland, G. G. W. Lee, S. M. Drew, K. R. Mann, K. A. McGee and S. C. Rasmussen, *Org. Lett.*, 2008, **10**, 1553–1556.
26 S. Yanagida, Y. Yu and K. Manseki, *Acc. Chem. Res.*, 2009, **42**, 1827–1838.
27 C.-Y. Chen, S.-J. Wu, C.-G. Wu, J.-G. Chen and K.-C. Ho, *Angew. Chem., Int. Ed.*, 2006, **45**, 5822–5825.
28 S. Caramori, S. Cazzanti, L. Marchini, R. Argazzi, C. A. Bignozzi, D. Martineau, P. C. Gros and M. Beley, *Inorg. Chim. Acta*, 2008, **361**, 627–634.
29 A. Grabulosa, M. Beley and P. C. Gros, *Inorg. Chim. Acta*, 2010, **363**, 1404–1408.
30 A. Monari, M. Beley, P. C. Gros and X. Assfeld, *J. Phys. Chem. A*, 2011, **115**, 3596–3603.
31 J. Preat, *J. Phys. Chem. C*, 2010, **114**, 16716–16725.
32 J. Preat, D. Jacquemin, C. Michaux and E. A. Perpète, *Chem. Phys.*, 2010, **376**, 56–68.
33 J. Preat, C. Michaux, D. Jacquemin and E. A. Perpète, *J. Phys. Chem. C*, 2009, **113**, 16821–16833.
34 M. Pastore and F. De Angelis, *ACS Nano*, 2010, **4**, 556–562.
35 F. De Angelis, S. Fantacci, A. Selloni, M. Grätzel and M. K. Nazeeruddin, *J. Am. Chem. Soc.*, 2007, **129**, 14156–14157.
36 S. Fantacci, F. De Angelis and A. Selloni, *J. Am. Chem. Soc.*, 2005, **125**, 16835–16847.

37 J. Nakazaki, I. Chung, M. M. Matsushita, T. Sugawara, R. Watanabe, A. Izuoka and Y. Kawada, *J. Mater. Chem.*, 2003, **13**, 1011–1022.
38 K. Ogura, R. Zhao, H. Yanai, K. Maeda, R. Tozawa, S. Matsumoto and M. Akazome, *Bull. Chem. Soc. Jpn.*, 2002, **75**, 2359–2370.
39 C. L. Fraser, N. R. Anastasi and J. J. S. Lamba, *J. Org. Chem.*, 1997, **62**, 9314–9317.
40 A. P. Smith, J. J. S. Lamba and C. L. Fraser, *Org. Synth.*, 2001, **78**, 82–90.
41 A. D. J. Becke, *Chem. Phys.*, 1993, **98**, 5648–5652.
42 R. B. R. Krishnan, J. S. Binkley, R. Seeger and A. J. Pople, *J. Chem. Phys.*, 1980, **72**, 650–654.
43 T. Yanai, D. Tew and N. Handy, *Chem. Phys. Lett.*, 2004, **393**, 51–57.
44 S. Miertus, E. Scrocco and J. Tomasi, *J. Chem. Phys.*, 1981, **55**, 117–129.
45 In order to get a more detailed description of the shorter wavelength region, a much higher number of states should be computed, thus leading to a significant increase in the computational cost.
46 Zinc–polypyridine complexes are known to display strong ILCT transitions and no MLCT due to the high third ionization potential of zinc and therefore are useful to identify ligand-based processesupon excitation in ruthenium complexes. See for example: T. Renouard and H. Le Bozec, *Eur. J. Inorg. Chem.*, 2000, 229–239.
47 T. H. Dunning Jr and P. J. Hay, in *Modern Theoretical Chemistry*, ed. H. F. Schaefer III, Plenum, New York, 1976, vol. 3, pp. 1–28.
48 J.-D. Chai and M. Head-Gordon, *Phys. Chem. Chem. Phys.*, 2008, **10**, 6615–6620.
49 A. Monari, T. Very, J.-L. Rivail and X. Assfeld, *Comput. Theor. Chem.*, 2011, DOI: 10.1016/j.comptc.2011.1011.1026.
50 S. Cazzanti, S. Caramori, R. Argazzi, C. M. Elliott and C. A. Bignozzi, *J. Am. Chem. Soc.*, 2006, **128**, 9996–9997.
51 M. J. Frisch, G. W. Trucks, H. B. Schlegel, G. E. Scuseria, M. A. Robb, J. R. Cheeseman, G. Scalmani, V. Barone, B. Mennucci, G. A. Petersson, H. Nakatsuji, M. Caricato, X. Li, H. P. Hratchian, A. F. Izmaylov, J. Bloino, G. Zheng, J. L. Sonnenberg, M. Hada, M. Ehara, K. Toyota, R. Fukuda, J. Hasegawa, M. Ishida, T. Nakajima, Y. Honda, O. Kitao, H. Nakai, T. Vreven, J. A. Montgomery, Jr., J. E. Peralta, F. Ogliaro, M. Bearpark, J. J. Heyd, E. Brothers, K. N. Kudin, V. N. Staroverov, R. Kobayashi, J. Normand, K. Raghavachari, A. Rendell, J. C. Burant, S. S. Iyengar, J. Tomasi, M. Cossi, N. Rega, J. M. Millam, M. Klene, J. E. Knox, J. B. Cross, V. Bakken, C. Adamo, J. Jaramillo, R. Gomperts, R. E. Stratmann, O. Yazyev, A. J. Austin, R. Cammi, C. Pomelli, J. Ochterski, R. L. Martin, K. Morokuma, V. G. Zakrzewski, G. A. Voth, P. Salvador, J. J. Dannenberg, S. Dapprich, A. D. Daniels, O. Farkas, J. B. Foresman, J. V. Ortiz, J. Cioslowski and D. J. Fox, *GAUSSIAN 09 (Revision A.1)*, Gaussian, Inc., Wallingford, CT, 2009.

